strument at 46.1 or 76.8 MHz, respectively. A spectral width of 20 000 Hz was typical using 8K data points. A prepulse delay of 500 μs to 50 ms was used. Signal to noise was improved as described for the proton spectra. For samples with intense diamagnetic resonances a Super-WEFT pulse sequence[46] was used.

Electron paramagnetic resonance spectra were collected using a Bruker ER 200 D spectrometer and 4-mm-o.d. quartz sample tubes. The composition of the EPR samples was confirmed by placing the EPR sample tube into an NMR tube and collecting the NMR spectra before and after the EPR measurement.

Abbreviations used: P, porphyrin dianion; P•, porphyrin π radical monoanion; TPP, tetraphenylporphyrin dianion; TMP, tetramesitylporphyrin dianion; *N*-MeTTP, *N*-methyltetra-*p*-tolylporphyrin monoanion; *N*-MeIm, *N*-methylimidazole.

Acknowledgment. We thank the National Institutes of Health (Grant GM26226) for support.

(46) Inubushi, T.; Becker, E. D. *J. Magn. Reson.* **1983**, *51*, 128.

Preparation and Characterization of Two New Group VI Quadruply Bonded Dinuclear Compounds: $Cr_2(DFM)_4$ and $W_2(DFM)_4$

F. Albert Cotton* and Tong Ren

Contribution from the Department of Chemistry and Laboratory of Molecular Structure and Bonding, Texas A&M University, College Station, Texas 77843. *Received August 20, 1991*

Abstract: Two new complexes, $Cr_2(DFM)_4$ (**1**) and $W_2(DFM)_4$ (**2**) (HDFM = di-*p*-tolylformamidine), have been synthesized to complete the triad of group VI dinuclear complexes with formamidine ligands. Direct interaction between $CrCl_2$ and LiDFM results in light yellow **1** (87%), which was crystallized as $Cr_2(DFM)_4 \cdot 2C_6H_6$ in space group *Pbnb* with a = 17.021 (3) Å, b = 24.266 (9) Å, c = 15.335 (3) Å, V = 6334 (3) Å^3, and Z = 4. The reaction between LiDFM and $Na_4(THF)_xW_2Cl_8$ affords orange **2**, which cocrystallizes with one toluene molecule in space group $P4/n$ with a = 13.259 (2) Å, c = 17.460 (3) Å, V = 3069 (1) Å^3, and Z = 2. The metal-metal distances determined through diffraction study are 1.930 (2) and 2.187 (1) Å for **1** and **2**, respectively. While the cycle voltammogram of **1** is featureless within the range of +1500 to −2500 mV, a reversible oxidation for **2** was recorded at a potential of −280 mV, which suggests the accessibility of the $W_2(DFM)_4^+$ species. The magnetic anisotropies of several known $M_2(DFM)_4$ type compounds are estimated from their ^1H NMR data. The electronic spectra of both **1** and **2** have been explained on basis of the previous theoretical study on $Mo_2(DFM)_4$.

Introduction

In the development of the chemistry of multiply bonded dimetal compounds,[1] especially those with quadrupole bonds, it has always been of particular interest to obtain homologous series of compounds with metal atoms from the first, second, and third transition series embraced by the same set of ligands. To do this, bridging bidentate ligands (generally represented LL) have been especially useful. The first such series comprised the 2-oxo-6-methylpyridinato (mhp^-) compounds, $M_2(mhp)_4$, with M = Cr, Mo, and W,[2] and only in group VI have such homologous series been obtained. Despite their rarity, such series are of special importance because of the insight they can provide into the factors that control M–M multiple bond stability.

A class of LL ligands that have gradually become more important in preparing a wide variety of $M_2(LL)_4$ compounds are those of general type $ArNXNAr^-$, where Ar is either phenyl or *p*-tolyl (tol) and X is N or CH, and a considerable numbers of $M_2(ArNXNAr)_4$ compounds,[3-6] with the metals Ni, Ru, Os, Rh, Pd, and Ir have been synthesized and structurally characterized by employing the ligand $[(tol)NCHN(tol)]^-$, abbreviated DFM for ditolylformamidine. $Mo_2(DFM)_4$ is the only such compound well characterized among the group VI elements.[7] The dichromium complex with a ligand similar to DFM^-, $Cr_2[HC(N\text{-}3,5\text{-}xylyl)_2]_4$, was synthesized earlier in a low yield (12%) by refluxing $Cr(CO)_6$ with neutral ligand for 18 days, but all attempts to grow suitable single crystals failed.[8] The molecular structure of the dichromium complex with another analogous ligand, *N*,*N*′-dimethylbenzamide, has also been determined, and this compound was one of the earliest examples of a "supershort" Cr–Cr bond (1.843 Å).[9]

Ditungsten complexes with metal–metal quadruple bonds are usually difficult to synthesize and manipulate, presumably because of the reactivity of the δ bond.[1b] The $W_2(LL)_4$ type complexes are only known for LL as carboxylates and hydroxypyridinate derivatives. Those ligands, as discussed in detail in the earlier studies of diruthenium(II) complexes, are relatively weak bases (poor in both σ and π donation). Hence, the isolation and characterization of a ditungsten(II) complex with a more basic ligand was considered a desirable objective in ditungsten chemistry.

In this report we describe the synthesis and molecular structure determination of both dichromium and ditungsten compounds with DFM. Some interesting spectroscopic and other physical properties will also be reported and discussed.

Experimental Section

All the syntheses and spectroscopic characterizations were carried out in argon atmosphere using standard Schlenkware. $CrCl_2$ was purchased

(1) Cotton, F. A.; Walton, R. A. *Multiple Bonds Between Metal Atoms*, 2nd ed.; Wiley: New York, 1982.
(2) Cotton, F. A.; Fanwick, P. E.; Niswander, R. H.; Sekustowski, J. C. *J. Am. Chem. Soc.* **1978**, *100*, 4725.
(3) (a) Cotton, F. A.; Matusz, M.; Poli, R. *Inorg. Chem.* **1987**, *26*, 1472. (b) Cotton, F. A.; Matusz, M.; Poli, R.; Feng, X. *J. Am. Chem. Soc.* **1988**, *110*, 1144.
(4) (a) Cotton, F. A.; Ren, T. *Inorg. Chem.* **1991**, *30*, 3675. (b) Cotton, F. A.; Ren, T.; Eglin, J. L. *Inorg. Chem.* **1991**, *30*, 2559.
(5) Piraino, P.; Bruno, G.; Schiavo, S. L.; Laschi, F.; Zanello, P. *Inorg. Chem.* **1987**, *26*, 2205.
(6) Cotton, F. A.; Poli, R. *Polyhedron* **1987**, *6*, 1625.
(7) Cotton, F. A.; Feng, X.; Matusz, M. *Inorg. Chem.* **1989**, *28*, 594.
(8) DerRoode, W. H.; Vrieze, K.; Koerner von Gustorf, E. A.; Ritter, A. *J. Organomet. Chem.* **1977**, *135*, 183.
(9) Bino, A.; Cotton, F. A.; Kaim, W. *Inorg. Chem.* **1979**, *18*, 1979.

0002-7863/92/1514-2237$03.00/0

from Alfa. WCl_4 and di-*p*-tolylformamidine (HDFM) were prepared according to the literature.[10,11] All solvents used were freshly distilled over suitable drying reagents under N_2.

Preparation of $Cr_2(DFM)_4$ (1). A three-neck round-bottom flask was charged with 0.49 g of $CrCl_2$ (4.0 mmol) and 10 mL of THF. To this pink-gray slurry was added 8.0 mmol of LiDFM in 30 mL of THF (prepared by neutralizing 1.8 g of HDFM with 5.0 mL of 1.6 M Li-*n*-Bu at −78 °C) via a cannula. The color of the mixture gradually turned to brown. After the mixture was stirred for 12 h, the volatiles were removed by vacuum distillation and the resulting yellow solid was washed with 3 × 20 mL of MeOH and then extracted with 80 mL of hot benzene. The benzene filtrate was orange, while some insoluble (in benzene, THF, and CH_2Cl_2) pale gray solid was left behind (it was dark green when wet). Upon washing of the residue with a large amount of distilled water in air on a frit, a small amount green gel was formed, which was readily dissolved in strong acid. The insoluble residue, based on the above observation, was assumed to be a mixture of LiCl and polymeric chromium(III) hydrate.[12] Freeze-drying of the benzene filtrate gave 1.73 g (87%) of a homogeneous yellow solid. Solutions of this complex are quite air-sensitive and became brown immediately on exposure to air. The solid sample could be handled in air quickly but gradually degraded to a sticky brown solid after sitting in the bench atmosphere for a few days. When **1** was dissolved in CH_2Cl_2 under an inert atmosphere, its yellow color steadily turned to brown over 2 days. Yellow needles, some of X-ray quality, were readily formed when a hexane/benzene mixture was allowed to stand for 1 week. UV/vis (toluene): 445 nm (1640 M^{-1} cm^{-1}), 294 (56 000). ^1H NMR (C_6D_6, ppm): 2.08 (s, CH_3), 6.34 and 6.80 (d, C_6H_4), 8.73 (s, NCHN).

Preparation of $W_2(DFM)_4$ (2). WCl_4 (1.30 g, 4.0 mmol) was suspended in 30 mL of THF, to which 4.0 mmol of Na in the form of amalgam was added at room temperature. The suspension became green in 20 min and was cooled to −30 °C. Addition of another 4 mmol of Na/Hg with vigorous stirring resulted in a royal blue solution in ca. 15 min, and 8.5 mmol of LiDFM in 15 mL of THF was introduced at this point. The reaction mixture was still blue when kept at −30 °C and became brown when allowed to warm slowly to room temperature. It was then refluxed for an additional 6 h. (Note: If LiDFM was added after the $W_2Cl_8^{4-}$ had decomposed into "WCl_2" at room temperature, only an intractable oily product could be isolated.) The dark brown reaction mixture was filtered through a Celite column to remove Hg, NaCl, and part of the LiCl. The solvent was removed from the filtrate via vacuum distillation to leave a dark residue, which was further heated at 100 °C for 4 h to ensure the complete removal of THF and then refluxed with 25 mL of MeOH for 1 h. After this mixture was cooled to room temperature, it was filtered through a fine frit. The orange solid collected on the frit was recrystallized from toluene. The orange crystalline material was dried under vacuum overnight to yield 1.14 g (45%) of a toluene-free (as evidenced by the ^1H NMR) sample. This compound is very air-sensitive in both solution and the solid state. All manipulations of the sample have to be done under an inert atmosphere. However, in contrast to the dichromium case, no decomposition was observed when this complex was dissolved in CH_2Cl_2. Also, this complex is inert toward deoxygenated water even under reflux. The single crystal used for X-ray diffraction study was grown by a slow diffusion of hexane into a saturated toluene solution. UV/vis (toluene): 443 nm (sh, ca. 11 880 M^{-1} cm^{-1}), 414 (12 360) 295 (49 040). ^1H NMR (C_6D_6, ppm): 2.06 (s, CH_3), 6.50 and 6.80 (d, C_6H_4), 8.65 (s, NCHN).

Physical Measurements. The UV/visible spectra were measured on a Cary 17D spectrometer at ambient temperature using a quartz cell (800–280 nm). ^1H NMR spectra were recorded on a Varian 200 spectrometer. Cyclic voltammetry measurements were carried out on a BAS 100 electrochemical analyzer in 0.2 M $(n\text{-Bu})_4NBF_4$ solution (**1** in THF and **2** in CH_2Cl_2) with a Pt working electrode and a Ag/AgCl reference electrode. Ferrocene was oxidized at 650 mV under the experimental conditions for **2**.

X-ray Crystallography. For **1** a golden needle was mounted on the top of a quartz fiber with epoxy resin and kept at −50 °C during the data collection. An orthorhombic cell was derived from the initial indexing and further confirmed by axial oscillation photographs. The space group was uniquely determined as *Pbnb* (nonstandard setting of No. 56) from the systematic absences. Diffraction data were collected on an Enraf-Nonius CAD-4 diffractometer using monochromated Mo Kα radiation. The description of the equipment and a detailed discussion of the normal crystallographic procedures we followed are presented elsewhere.[13,14]

Table I. Crystallographic Parameters for $Cr_2(DFM)_4 \cdot 2C_6H_6$ and $W_2(DFM)_4 \cdot C_7H_8$

chemical formula	$Cr_2N_8C_{72}H_{72}$	$W_2N_8C_{67}H_{78}$
formula weight	1153.2	1353.0
space group	*Pbnb* (No. 56)	*P4/n*
a, Å	17.021 (4)	13.259 (2)
b, Å	24.266 (11)	
c, Å	15.335 (4)	17.460 (3)
V, Å^3	6334 (3)	3069 (1)
Z	4	2
d_{calc}, g cm^{-3}	1.21	1.464
μ, cm^{-1} (M)	3.8 (Mo)	72.4 (Cu)
λ(Kα), Å (M)	0.710 73 (Mo)	1.541 84 (Cu)
data collection instrument	Enraf-Nonius CAD-4	AFC5R Rigaku
T, °C	−50 ± 1	20 ± 1
transmissn coeff: max, min	1.00, 0.95	1.00, 0.57
R^a	0.070	0.046
R_w^b	0.074	0.049

$^a R = \sum||F_o| - |F_c||/\sum|F_o|$. $^b R_w = [\sum w(|F_o| - |F_c|)^2/\sum w|F_o|^2]^{1/2}$; $w = 1/\sigma^2(|F_o|)$.

The data set was corrected for Lorentz and polarization effects. There was no observable decay during the data collection. An empirical absorption correction based on the ψ-scan method was also applied to the data.[15]

This compound crystallized in a phase which is isomorphous to that for $Ru_2(DFM)_4(C_6H_6)_2$.[4] The refined coordinates and thermal parameters for $Ru_2(DFM)_4$ (not including the solvent molecule) were therefore used as the starting model, and refinement converged smoothly. A difference Fourier map at this stage had its first 12 peaks arranged as two six-membered rings overlapped with each other; this pattern was interpreted as a benzene molecule disordered by a slight dislocation. These peaks were then refined to convergence in SHELX-76 as two independent rigid-body hexagons with one isotropic thermal parameter for each hexagon, and the sum of site occupancies for the two hexagons was set to unity (converged site occupancies are 57% and 43%). The final difference Fourier map was featureless with the highest peak (0.55 e/Å^3) as a ghost peak of Cr.

For **2**, an orange-red plate of dimensions 0.45 × 0.15 × 0.06 mm^3 was protected under a mixture of mother liquor and deoxygenated mineral oil in a Lindemann capillary. Initial indexing based on 14 reflections within the range of 38° ≤ 2θ ≤ 42 ° resulted in a tetragonal cell, while the Laue symmetry 4/*m* was confirmed by oscillation photographs and the space group was unambiguously assigned as P4/*n* from the systematic absences observed in the diffraction data. Diffraction data were collected on an AFC5R Rigaku diffractometer using monochromated Cu Kα radiation. The data set was corrected for the effects of Lorentz, polarization and decay (overall change in intensity during the period of data collection was −22.2%), and absorption (based on the ψ-scan method).

The positions of the W atoms and the atoms of their first coordination shell as well were derived by analyzing a three-dimensional Patterson map and further refined with isotropic thermal parameters. The rest of the non-hydrogen atoms in the molecule were found by routine methods of alternate difference Fourier maps and least-squares refinements. A difference Fourier map at the convergence of anisotropic refinement of the molecule revealed the peaks of a toluene molecule, which resided on the 4-fold axis and was thus disordered by a C_4 operation. The methyl group was also disordered over both ends of the molecule. Further refinement was carried out in SHELX-76 with constraint on all independent interatomic distances of the toluene molecule. The final figures of merit and other related crystallographic parameters for both **1** and **2** are collected in Table I, and the fractional coordinates of all atoms for **1** and **2** are listed in the supplementary material.

Results and Discussion

Chemistry. While the previous preparation of a Cr_2(formamidinato)$_4$ compound by refluxing $Cr(CO)_6$ with the neutral ligand was lengthy and gave a low yield,[8] we demonstrate here that $Cr_2(DFM)_4$ can be prepared with the yield as high as 87%. It is most likely that the formation of LiCl from the chloride in the anhydrous $CrCl_2$ is the main driving force for such a clean reaction. Failure to obtain high-quality crystals from refluxing

(10) Roberts, R. M. *J. Org. Chem.* **1949**, *14*, 277.
(11) Schrock, R. R.; Sturgeoff, L. G.; Sharp, P. R. *Inorg. Chem.* **1983**, *22*, 2801.
(12) Cotton, F. A.; Wilkinson, G. *Advanced Inorganic Chemistry*, 5th ed.; Wiley: New York, 1988; p 687.
(13) Bino, A.; Cotton, F. A.; Fanwick, P. E. *Inorg. Chem.* **1979**, *18*, 3558.
(14) Cotton, F. A.; Frenz, B. A.; Deganello, G.; Shaver, A. *J. Organomet. Chem.* **1973**, *50*, 227.
(15) North, A. C. T.; Phillips, D. C.; Mathews, F. S. *Acta Crystallogr., Sect. A: Cryst. Phys., Diffr., Theor. Gen. Crystallogr.* **1968**, *24A*, 351.

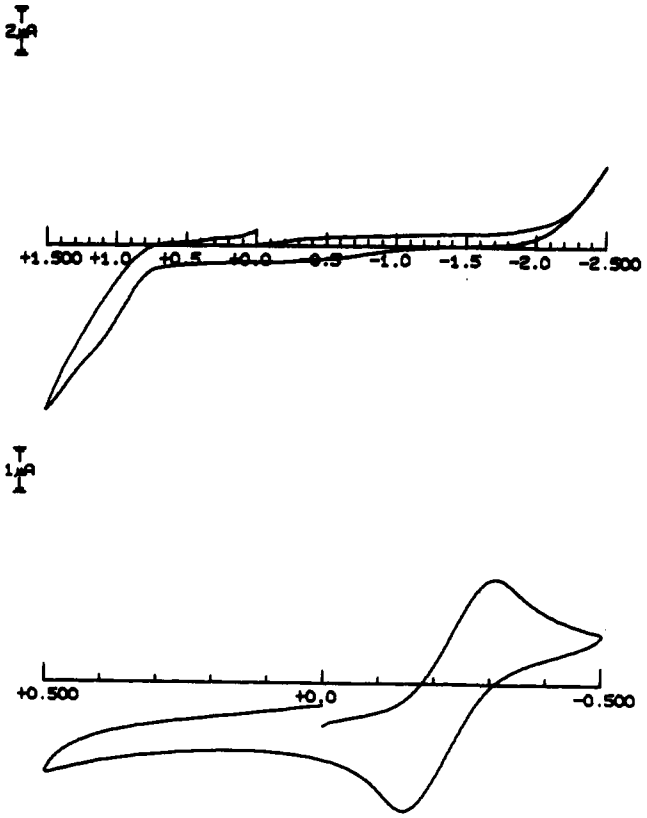

Figure 1. Cyclic voltammograms of $Cr_2(DFM)_4$ (a, top) and $W_2(DFM)_4$ (b, bottom).

$Cr(CO)_6$ is probably an indication of insufficient purity of the product.

There is no obvious color change when solutions of **1** in either benzene or THF are kept under an argon atmosphere. In contrast to the earlier claim of dinuclear–mononuclear equilibrium in solution,[8] the well-resolved sharp ^1H NMR spectrum of **1** in C_6D_6 clearly indicates the integrity of the dinuclear structure in solution, since the mononuclear Cr(II) species is a high-spin (d^4) center, which would cause both an upfield shift and a dramatic peak broadening in the ^1H NMR. The decomposition of **1** in CH_2Cl_2 is presumably due to the oxidative addition to the dichromium core, perhaps to afford the edge-sharing bioctahedral dichromium(III) complex on the right side of the following equation.

$$Cr_2(DFM)_2 + CH_2Cl_2 \rightarrow Cr_2(\mu\text{-}Cl)_2(\mu\text{-}DFM)_2(\eta^2\text{-}DFM)_2$$

Similar oxidative addition of hydroxyl groups might be responsible for the decomposition of **1** in the laboratory atmosphere.

In an earlier attempt to synthesize a ditungsten complex with –NCN– bridging groups by refluxing $W(CO)_6$ with *N,N'*-diphenylbenzamide, only the formation of (arene)$W(CO)_3$ was observed.[16] Similarly, refluxing $W(CO)_6$ with various formamidines yielded a purple species,[8] which was identified later[17] as $W_2(\mu\text{-}CO)_2(\mu\text{-form})_2(\eta^2\text{-form})_2$. Since the high-yield synthesis of **1** was attributed to the formation of LiCl, we anticipated that a good synthesis of the homologous tungsten compound could be developed by reacting LiDFM with a well-known tungsten(II) chloride source, Schrock's $Na_4(THF)_xW_2Cl_8$.[11,18] Although the yield is not very high, it is still a practical preparation in view of the availability of WCl_4. The purity of the product is attested by the satisfactory ^1H NMR spectrum and the successful crystallization of **2**. It is also notable that **2** can only be obtained by starting from $W_2Cl_8^{4-}$, rather than "WCl_2".

As shown by its cyclic voltammogram in Figure 1a, **1** does not have any reversible reduction or oxidation in the range +1500 to −2500 mV (vs. Ag/AgCl). The tail close to the positive end probably corresponds to a decomposition of the compound. This indicates that removal of a δ electron induces the collapse of the quadruply bonded dichromium compound. This could be because the stability of the octahedral, t_{2g}^3 Cr^{3+} ion is very great. The cyclic voltammogram of the W compound (Figure 2b) consists of a single standard reversible oxidation at −228 mV (i_c/i_a = 1.05), which is about 200 mV lower than that recorded for $Mo_2(DFM)_4$. This difference is consistent with the well-established easier oxidizability of the W_2^{4+} center compared to the Mo_2^{4+} center. The reversible oxidation for both the Mo and W compounds shows that the strong π and σ bonding in both enables the structures to survive one-electron oxidation.

Molecular Structures. $Cr_2(DFM)_4$ (1). An ORTEP drawing of the molecule is shown in Figure 2, while the most interesting bond lengths and angles are collected in Table II. The overall geometry of the molecule, the bidentate bridging structure, is similar to all of those previously observed for $M_2(DFM)_4$ units. Compound **1** has a rigorous C_2 axis coinciding with the Cr–Cr vector. The first coordination shell of the dichromium core is slightly twisted

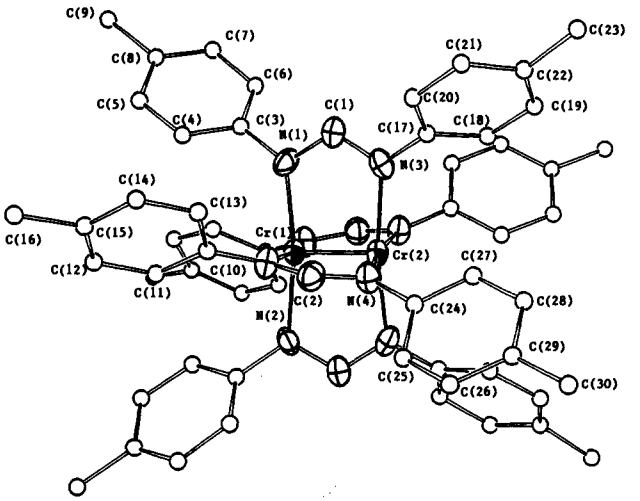

Figure 2. ORTEP drawing of $Cr_2(DFM)_4$ at 50% probability level. The carbon atoms of the tolyl groups are drawn with arbitrary radii for clarity.

Table II. Selected Bond Distances (Å) and Angles (deg) for $Cr_2(DFM)_4 \cdot 2C_6H_6$[a]

Bond Distances			
Cr(1)–Cr(2)	1.930 (2)	N(2)–C(2)	1.33 (1)
Cr(1)–N(1)	2.053 (7)	N(2)–C(10)	1.41 (1)
Cr(1)–N(2)	2.059 (7)	N(3)–C(1)	1.32 (1)
Cr(2)–N(3)	2.050 (7)	N(3)–C(17)	1.41 (1)
Cr(2)–N(4)	2.026 (7)	N(4)–C(2)	1.36 (1)
N(1)–C(1)	1.34 (1)	N(4)–C(24)	1.41 (1)
N(1)–C(3)	1.42 (1)		

Bond Angles			
Cr(2)–Cr(1)–N(1)	94.9 (2)	Cr(1)–N(1)–C(3)	128.7 (6)
Cr(2)–Cr(1)–N(2)	94.6 (2)	Cr(1)–N(2)–C(2)	115.0 (6)
N(1)–Cr(1)–N(1)	170.2 (3)	Cr(1)–N(2)–C(10)	128.0 (6)
N(2)–Cr(1)–N(2)	170.8 (3)	Cr(2)–N(3)–C(1)	115.4 (6)
Cr(1)–Cr(2)–N(3)	94.8 (2)	Cr(2)–N(3)–C(17)	127.9 (6)
Cr(1)–Cr(2)–N(4)	95.4 (2)	Cr(2)–N(4)–C(2)	115.3 (5)
N(3)–Cr(2)–N(3)	170.5 (3)	Cr(2)–N(4)–C(24)	128.5 (6)
N(4)–Cr(2)–N(4)	169.2 (3)	N(1)–C(1)–N(3)	119.4 (8)
Cr(1)–N(1)–C(1)	114.4 (6)	N(2)–C(2)–N(4)	118.6 (7)

[a] Numbers in parentheses are estimated standard deviations in the least significant digits.

(16) Cotton, F. A.; Inglis, T.; Kilner, M.; Webb, T. R. *Inorg. Chem.* **1975**, *14*, 2023.
(17) Schagen, J. D.; Schenk, H. *Cryst. Struct. Commun.* **1978**, *7*, 223.
(18) (a) Sharp, P. R.; Schrock, R. R. *J. Am. Chem. Soc.* **1980**, *102*, 1430. (b) Cotton, F. A.; Mott, G. N.; Schrock, R. R.; Sturgeoff, L. G. *J. Am. Chem. Soc.* **1982**, *104*, 6781.

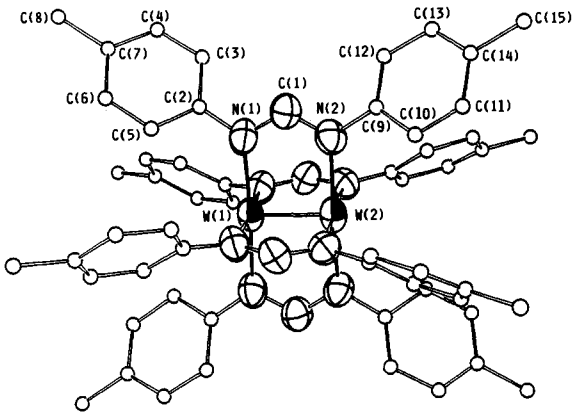

Figure 3. ORTEP drawing of $W_2(DFM)_4$ at 50% probability level. The carbon atoms of the tolyl groups are drawn with arbitrary radii.

Table III. Selected Bond Distances (Å) and Angles (deg) from $W_2(DFM)_4 \cdot C_7H_8$[a]

Bond Distances			
W(1)–W(2)	2.187 (1)	N(1)–C(2)	1.40 (2)
W(1)–N(1)	2.13 (1)	N(2)–C(1)	1.34 (2)
W(2)–N(2)	2.14 (1)	N(2)–C(9)	1.44 (2)
N(1)–C(1)	1.34 (2)		
Bond Angles			
W(2)–W(1)–N(1)	91.8 (2)	W(1)–N(1)–C(2)	125.0 (8)
N(1)–W(1)–N(1)	176.5 (3)	W(2)–N(2)–C(1)	119.2 (8)
W(1)–W(2)–N(2)	91.2 (2)	W(2)–N(2)–C(9)	124.7 (8)
N(2)–W(2)–N(2)	177.7 (3)	N(1)–C(1)–N(2)	119. (1)
W(1)–N(1)–C(1)	118.9 (8)		

[a] Numbers in parentheses are estimated standard deviations in the least significant digits.

from a perfectly eclipsed configuration by torsional angles N(1)–Cr(1)–Cr(2)–N(3) and N(2)–Cr(1)–Cr(2)–N(4) of 8.4 (3)° and 8.7 (3)°, respectively. The average Cr–N distance (2.047 [7] Å) is within the 3σ range of that for $Cr_2(N,N'$-dimethylbenzamidinato)$_4$ (2.032 [5] Å), consistent with the similar basicities of the two ligands.

The most important dimension of **1** is, of course, the Cr–Cr distance (1.930 (2) Å), which is 0.087 Å longer than that of the analogous complex $Cr_2(N,N'$-dimethylbenzamidinato)$_4$ (1.843 Å), and 0.03 Å out of the range of so-called supershort (≤1.90 Å) Cr–Cr quadruple bond. The difference here could be mainly due to the reduction of the "bite" (the spacing between the two coordinating nitrogen atoms of the ligand) in the latter due to the steric interaction between the *N*-methyl and the phenyl group in the middle. While an explicit value for the "bite" is not available from the reference, it can be inferred from the angle N–C–N, which is 116.3 [5]° for the previous complex and 119.0 [8]° for **1**.

$W_2(DFM)_4$ (2). The molecular structure is best represented by a perspective view in Figure 3. This molecule also shows a great resemblance to other $M_2(DFM)_4$ molecules. It has a crystallographically imposed C_4 symmetry with both W atoms residing on the 4-fold axis. The molecule has effective D_{4h} point symmetry with only a small deviation; viz., N(1)–W(1)–W(2)–N(2) = 2.8 (0.4)°. The average of the two almost identical W–N distances is 2.135 [10] Å, which is about 0.09 Å longer than the Cr–N bond length in **1** and, surprisingly, 0.04 Å shorter than the Mo–N bond length in $Mo_2(DFM)_4$. When the differences in the covalent radii[19] (Cr, 1.186 Å; Mo, 1.296 Å; W, 1.304 Å) are taken into account, the W–N is actually the "shortest" and implies a strong W–N interaction. Selected bond distances and angles are collected in Table III.

The crystal structure of **2** is isotypic to the one for $Mo_2(DFM)_4$, with the *a* axis a little shorter and the unique axis significantly longer (0.582 Å). As shown by a packing diagram of **2** in Figure 4, the toluene molecule occupying the hole existing in the structure of the Mo analogue is responsible for this elongation. This raises the question of whether a highly disordered THF was present in that hole in the previous structure.

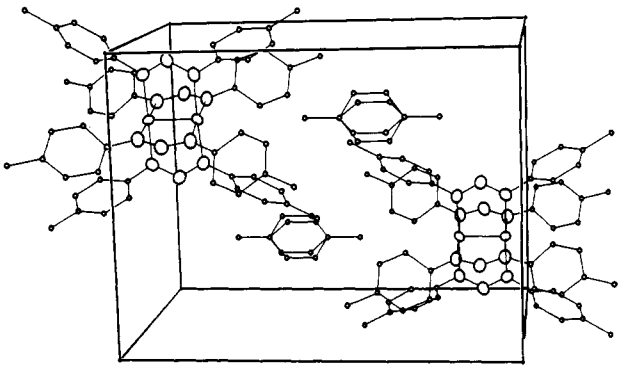

Figure 4. Packing diagram of $W_2(DFM)_4C_7H_8$. The disordered toluene is also shown. The view is along the *a* axis.

The 30 known quadruply bonded ditungsten complexes can be divided into three groups according to the ligand type and W–W distances as well: (a) $W_2(LL)_4$ with LL being the carboxylates and substituted hydroxypyridinates, with W–W bond lengths in the range of 2.155–2.246 Å; (b) homoleptic complexes $W_2X_8^{4-}$ with X = Me and Cl, and a W–W range of 2.254–2.264 Å; (c) $W_2P_4Cl_4$ with P_4 as either four monodentate phosphines or two bidentate phosphines, where the range is 2.26–2.32 Å. Our new complex, $W_2(DFM)_4$, falls into the first group with a short W–W quadruple bond, 2.187 (1) Å.

An interesting feature of this homologous series of $M_2(DFM)_4$ compounds is the closeness of the FSRs, formal shortness ratio,[1] defined for a bond A–B as

$$FSR_{AB} = D_{A\text{-}B}/(R_1^A = R_1^B)$$

which can be calculated from the Pauling R_1s as 0.814 (Cr), 0.804 (Mo), and 0.838 (W). The other series having close FSRs is the 6-methylhydroxypyridinate compounds which have 0.796 for Cr, 0.797 for Mo, and 0.829 for W.[20] If the shortness of the metal–metal bond is due to the constraint of the pyridine ring in the latter series,[21] such a constraint apparently does not exist for the ligands like formamidine, since it is known that the bridging bidentate structure was assumed by $Ag_2(DFM)_2$ with an Ag–Ag separation as great as 2.705 Å.[22] Therefore, the formation of the metal–metal quadruple bonds is solely responsible for the small FSRs in this series.

NMR Spectra. The proton NMR spectra of both **1** and **2** are typical for all these diamagnetic $M_2(DFM)_4$ compounds: a singlet upfield for the methyl group, two doublets arranged in an approximate AB spectrum for C_6H_4, and a singlet most downfield for the methine hydrogen because of the very large magnetic anisotropy of the M–M quadruple bond. Since there are enough NMR data available for the $M_2(DFM)_4$ type compounds, it is possible to estimate the magnetic anisotropies based on the change of the chemical shifts, especially the change of the methine proton, which is fixed right over the center of M–M bond, while positions of other protons are changing all the time in solution due to the free rotation of the tolyl group. The change of chemical shift is related to the magnetic anisotropy by the McConnell equation:[22]

$$\Delta\delta = \Delta\chi[(1 - 3\cos^2\theta)/12\pi r^3]$$

Here, $\Delta\delta$ is the change of chemical shift (ppm), r is the length (Å) of the vector from the center of the metal–metal bond to the proton, θ is the angle between the vector r and the bond axis, and $\Delta\chi = \chi_\parallel - \chi_\perp$ is the magnetic anisotropy (units 10^{-36} m^3/mole-

(19) Pualing, L. *The Nature of the Chemical Bond, 3rd* ed.; Cornell University Press: Ithaca, NY, 1960; p 403.

(20) Cotton, F. A.; Fanwick, P. E.; Niswander, R. H.; Sekutowski, J. C. *J. Am. Chem. Soc.* **1978**, *100*, 4725.

(21) Edema, J. J. H.; Gambarotta, S. *Comments Inorg. Chem.* **1991**, *11*, 195.

(22) Harris, R. K. *Nuclear Magnetic Resonance Spectroscopy*; Pittman: London, 1983; p 194.

Table IV. Magnetic Anisotropies for Several $M_2(DFM)_4$ Complexes

metal	Ni	Cr	Mo[a]	W	Re[b]	Ru[c]
δ (ppm)	6.16	8.73	8.42	8.65	8.32	8.11
$\Delta\delta$		2.57	2.26	2.49	2.16	1.95
r (Å)		3.78	3.89	3.88	3.79	3.72
$\Delta\chi$[d]		5230	5020	5480	4430	3780

[a] Reference 6. [b] Reference 27. The molecular formula is $Re_2(DFM)_4Cl_2$. [c] Reference 3. [d] In units of 10^{-36} m^3/molecule.

cule). The distance r of the methine proton can be readily calculated by adding 1.07 Å, the normal C–H distance in an olefin, to the distance of the methine carbon from the center of the metal–metal bond. The θ angles are very close to 90° and were all assumed to be 90°. Now the key problem is how to determine the change of chemical shift. In contrast to the previous calculations for the $M_2P_4X_4$ type complex,[23-25] the chemical shift of the free ligand HDFM cannot be taken as the standard, because the coordinated DFM is an anion, and thus the chemical environment of the methine proton has been dramatically changed even without magnetic anisotropy from the metal–metal multiple bond. However, the proton NMR spectra for $M_2(DFM)_4$ with M = Ni and Pd were studied in this laboratory.[26] In these compounds both molecular and electronic structures indicated that there are no bonding interactions between two metal centers. Therefore, the chemical shift of the methine proton for the Ni complex can be used as the "zero" point. (The chemical shift for the Pd complex is shifted slightly downfield, possibly due to some small magnetic anisotropy from the nonbonding interaction between two Pd atoms.) The δ of each methine proton, the $\Delta\delta$, the r value estimated based from the crystallographic data, and the magnetic anisotropy calculated thereby according to the McConnell equation are listed in Table IV for several $M_2(DFM)_4$ complexes.

There are a few unexpected results in Table IV: The magnetic anisotropy of the Mo compound is the smallest among the triad, even though it has the strongest quadruple bond in view of its smallest FSR. The magnitude derived here is about the same as those previously derived for $Mo_2P_4X_4$ type complexes from this laboratory,[23,25] although a little smaller due to the difference in the electronic structures. The anisotropy published for $W_2Cl_4(dippp)_2$[25] is incorrect because the formula on which the calculation was based was wrong. The magnitude of the $\Delta\chi$ for the diruthenium(II) compound is also comparable with those for the group VI compounds. This is interesting since the net metal–metal π bond order is zero because of the ground-state configuration $\delta^2\pi^4\sigma^2\pi^{*4}$.[4a] The $Re_2(DFM)_4Cl_2$ molecule,[27] though possessing a metal–metal quadruple bond, has a much smaller magnetic anisotropy than all the group VI compounds. Because data of this kind for both diruthenium(II) and dirhenium(III) species are rare (unprecedented to our knowledge), detailed explanation should await more efforts in the measurements of other analogous compounds and accurate theoretical calculations as well.

Electronic Spectra and Electronic Structures. The global electronic structures of both **1** and **2** are the same as that of $Mo_2(DFM)_4$; i.e., they have a $\sigma^2\pi^4\delta^2$ ground-state configuration (quadruple-bond configuration) based on the homology in the molecular structures. It is interesting to note that while in the diruthenium(II) and diosmium(III) cases M–M distances are dramatically elongated when the bridging carboxylate is replaced by more basic ligands such as triazene and formamidine, M–M distances in dinuclear complexes of group VI are insensitive to such a substitution. This clearly shows that the basicity of the bridging ligand has much less influence on the metal–metal bonding orbitals than on the antibonding orbitals.

Although additional calculations would surely provide more quantitative information, we can base a discussion on the available $X\alpha$ calculation for $Mo_2(DFM)_4$.[7] We shall address a few pertinent problems in both the electronic structures and electronic spectra of **1** and **2** qualitatively and refer to the results of the previous $X\alpha$ calculation for the Mo analogue wherever neccessary.

There is no question about the δ orbital being the HOMO in each case. The relative order of the HOMOs among the triad appears to be Mo < Cr < W. Since the W complex is so vulnerable to one-electron oxidation, its HOMO must be of high energy. The order between Mo and Cr is justified according to the FRSs, which indicate a less effective δ-type overlap between chromium atoms. Although the best overlap might be expected between two W atoms due to their more diffuse d orbitals, the δ bond between W atoms should also be weaker due to the inherent character of third transition series—the relativistic effect, which enables a better match in energy between the d_{xy} orbital and the antibonding orbital of the NCHN fragment and hence a larger antibonding component as compared with the $2b_{1u}$ orbital in $Mo_2(DFM)_4$.

Due to the π-basicity effect documented in the earlier study of the diruthenium analogue,[4] the order of the empty molecular orbitals for these $M_2(DFM)_4$ compounds cannot necessarily be assumed to be the same as those of both carboxylates and hydroxypyridinates. While the order of empty orbitals in **1** might still be expected to be the same as in the Mo case, with δ^* as the LUMO and π^* as the next virtual orbital, an inversion of the order between π^* and δ^* could occur in the W compound. As shown in the following discussion, the δ–δ^* transitions for both the Mo and W compounds have substantially higher energies than their counterparts with either carboxylate or hydroxypyridinate ligands.

The electronic spectrum of **1** bears an amazing similarity to that of $Mo_2(DFM)_4$. The $\delta \rightarrow \delta^*$ transition occurs as a well-resolved peak at 445 nm, the wavelength where the same transition was recorded for the Mo compound. This band is very weak because the intensity of the $\delta \rightarrow \delta^*$ transition will be proportional to the percentage of ligand mixing in both orbitals, and that is apparently very small for the Cr compound. However, it is uncertain why the $\delta \rightarrow \delta^*$ transition has same energy for both Cr and Mo. A strong charge-transfer band assigned as an $n \rightarrow \pi^*$ transition is also observed at a lower energy (294 nm).

The spectrum of the tungsten compound also has a charge-transfer band at 295 nm. The red-shift in energy can also be explained by a relativistic effect, which increases the mixing between π^*(core) and the *bonding* orbital of the NCHN fragment to give a π^* orbital of lower energy than that in the Mo compound. In support of this is the significant decrease in the extinction coefficient ϵ from 65 000 (Mo) to 49 000 (W).

As encountered in the case of $W_2(xhp)_4$ (xhp = mhp, fhp),[28] a compound peak was found between 400 and 450 nm for **2**. For xhp complexes, this peak was resolved by deconvolution into a weak band at lower energy which was assigned as the $\delta \rightarrow \delta^*$ transition and a much stronger peak at higher energy which was assigned as $\delta \rightarrow \pi_L^*$. However, we believe the nature of this band in **2** is quite different for two reasons. First, there is no ligand-based orbital which is accessible in the UV/vis range according to the model $X\alpha$ calculation for the Mo analogue. Second, the upward shift in the energy of the δ^* orbital in the W compound should exceed that of the δ orbital, thus resulting in a larger δ–δ^* gap than in the Mo case, a trend we discussed previously in the study of $Os_2(DFM)_4Cl_2$.[4b] Therefore, the peak centered at 414 nm is tentatively assigned as the real $\delta \rightarrow \delta^*$ transition. The large extinction coefficient can also be attributed to a much larger ligand contribution to the δ-type molecular orbitals. Considering the large spin–orbit coupling that prevails in the third transition series, we can assign the weaker transition centered at 443 nm as the spin-forbidden (singlet to triplet) sibling of one of the several possible dipole-allowed transitions which contribute to the strong charge-transfer band at 295 nm ($n \rightarrow \delta^*$, $n \rightarrow \pi^*$).

(23) (a) Cotton, F. A.; Kitagawa, S. *Inorg. Chem.* **1987**, *26*, 3463. (b) *Polyhedron* **1988**, *7*, 1673.
(24) Fryzuk, M. D.; Kreiter, C. G.; Sheldrick, W. S. *Chem. Ber.* **1989**, *122*, 851.
(25) Chen, J.-D.; Cotton, F. A.; Falvello, L. R. *J. Am. Chem. Soc.* **1990**, *112*, 1076.
(26) Cotton, F. A.; Matusz, M.; Poli, R.; Feng, X. *J. Am. Chem. Soc.* **1988**, *110*, 1144.
(27) Cotton, F. A.; Ren, T. *J. Am. Chem. Soc.* In press.
(28) Cotton, F. A.; Falvello, L. R.; Han, S.; Wang, W. *Inorg. Chem.* **1983**, *22*, 4106.

Concluding Remarks. New synthetic strategies have been developed for the dichromium(II) and ditungsten(II) complexes with ligands containing the very basic bridging group -NCHN-. Extensive application to the tungsten system may be expected since this is the first successful isolation of such a ditungsten(II) complex. The metal-metal quadruple bond is well established on the basis of the molecular structure and consistent spectroscopic data. The accessibility of the cation $W_2(DFM)_4^+$ is clearly suggested by the electrochemical study, and attempts to isolate it will be undertaken.

Acknowledgment. We are grateful to the National Science Foundation for support. We also acknowledge helpful comments about the crystallography from Drs. M. Shang and L. M. Daniels.

Supplementary Material Available: Complete tables of crystal data, positional parameters, bond distances and angles, and anisotropic displacement parameters for structures **1** and **2** (19 pages); listing of observed and calculated structure factors (19 pages). Ordering information is given on any current masthead page.

Antibody Targeting to Bacterial Cells Using Receptor-Specific Ligands

Carolyn R. Bertozzi and Mark D. Bednarski*

Contribution from the Department of Chemistry, University of California, Berkeley, California 94720. *Received July 26, 1991*

Abstract: The binding of antibodies to bacterial cells is necessary to effect host defense mechanisms such as complement activation and macrophage recognition. We have designed a biotinylated *C*-glycoside of mannose (BCM) that, when complexed with avidin, targets antibodies to a pathogenic strain of *Escherichia coli* containing type 1 pili mannose-specific receptors. Antibody binding to the bacterial cells was viewed by transmission electron microscopy using a protein A gold label. Antibody binding occurs only in the presence of the BCM-avidin conjugate and can be titrated off the surface of the cell by methyl α-D-mannopyranoside, demonstrating that antibody binding is mediated by the receptor. The conserved binding domain of cell-surface lectins can therefore be utilized to direct antibodies to pathogens.

Introduction

The binding of antibodies to antigenic determinants on the surface of a bacterial pathogen is required to activate pathways in humoral and cellular immunity.[1-4] The process of antibody-mediated cell toxicity includes complement activation (classical pathway) and opsonization for macrophage-mediated endocytosis along with direct recognition of the antibody-coated bacterium by macrophage Fc receptors.[5,6] Several strains of enterobacteria, such as *Escherichia*, *Klebsiella*, *Shigella*, and *Salmonella*, have proteinaceous appendages called pili (or fimbriae) that are located on the surface of the organism and provide antigenic recognition sites for the host's immune system.[4,7] Type 1 pili also contain receptors specific for terminal α-linked mannosides which mediate the adhesion of bacteria to host cells, a process that is essential for infectivity.[8-14] Many bacterial lectins, however, undergo rapid genetic changes to evade the host's immune system. Despite these genetic changes, the biological function and thus the binding specificity of bacterial cell-surface lectins are conserved.[4] We describe herein a strategy to target antibodies to a pathogenic strain of *Escherichia coli* K1 by exploiting the ligand specificity of the conserved type 1 pili mannose-specific receptors.

Both complement factor C1q and macrophage cells recognize an antibody-coated particle by interacting with the Fc region of the antibodies. Capon et al. and Traunecker et al. have shown that genetically engineered proteins in which the binding determinants of IgG or IgM molecules are replaced with CD4 can be used to target the Fc region to HIV-infected cells.[15,16] Shokat and Schultz have recently demonstrated that antibodies can be directed to purified HIV glycoprotein gp120 via 2,4-dinitrophenol conjugates of CD4 in vitro.[17] We report here that (1) the conjugate of a biotinylated *C*-glycoside of mannose (BCM; Figure 1) with avidin can mediate the attachment of anti-avidin antibodies to bacterial cells through the type 1 pili mannose-specific receptors and (2) the antibody binding event can be directly assayed using transmission electron microscopy (TEM) on whole bacterial cells. Since this approach to antibody targeting does not involve molecular cloning, it can be applied to other pathogenic organisms for which the cell-surface receptors bind to small molecules. Furthermore, the antibody binding event is visualized directly on the surface of the cell rather than on a purified receptor. Direct observation of antibody-coated pathogens by TEM should provide

(1) Joiner, K. A.; Brown, E. J.; Frank, M. M. *Annu. Rev. Immunol.* **1984**, *2*, 461.
(2) Soderstrom, T.; Ohman, L. *Scand. J. Immunol.* **1984**, *20*, 299.
(3) Ofek, I.; Sharon, N. *Infect. Immun.* **1988**, *56*, 539.
(4) Virji, M.; Heckels, J. E. *Infect. Immun.* **1985**, *49*, 621.
(5) Reid, K. B. M.; Porter, R. R. *Annu. Rev. Biochem.* **1981**, *50*, 433.
(6) Silverstein, S. C.; Steinman, R. M.; Cohn, Z. A. *Annu. Rev. Biochem.* **1977**, *46*, 669. Duncan, A. R.; Woof, J. M.; Partridge, L. J.; Burton, D. R.; Winter, G. *Nature* **1988**, *332*, 563.
(7) Clegg, S.; Gerlach, G. F. *J. Bacteriol.* **1987**, *169*, 934.
(8) Firon, N.; Ofek, I.; Sharon, N. *Infect. Immun.* **1984**, *43*, 1088.
(9) Firon, N.; Ofek, I.; Sharon, N. *Carbohydr. Res.* **1983**, *120*, 235.
(10) Ofek, I.; Mirelman, D.; Sharon, N. *Nature* **1977**, *265*, 623.
(11) Eshdat, Y.; Ofek, I.; Yashouv-Gan, Y.; Sharon, N.; Mirelman, D. *Biochem. Biophys. Res. Commun.* **1978**, *85*, 1551.
(12) Hanson, M. S.; Brinton, C. C., Jr. *Nature* **1988**, *332*, 265.
(13) Hanson, M. S.; Hempel, J.; Brinton, C. C., Jr. *J. Bacteriol.* **1988**, *170*, 3350.
(14) Bloch, C. A.; Orndorff, P. E. *Infect. Immun.* **1990**, *58*, 275.
(15) Capon, D. J.; et al. *Nature* **1989**, *337*, 525. Byrn, R. A.; et al. *Nature* **1990**, *344*, 667.
(16) Traunecker, A.; Schneider, J.; Kiefer, H.; Karjalainen, K. *Nature* **1989**, *339*, 68.
(17) Schultz, P. G.; Shokat, K. *J. Am. Chem. Soc.* **1991**, *113*, 1861.

0002-7863/92/1514-2242$03.00/0